Greenland Observed at High Resolution by the Seasat Scatterometer

D.G. Long[1], P.J. Hardin[2], and R.A. Shaw[3]

Brigham Young University
459 Clyde Building
Provo, Utah 84602

[1] Department of Electrical and Computer Engineering, [2] Department of Geography, [3] Department of Physics

ABSTRACT

The *Ku*-band (14.6 Ghz) Seasat scatterometer (SASS), which flew for 3 months in 1978, was designed to measure the normalized radar backscatter coefficient (σ^o) of the Earth's surface for the purpose of estimating near-surface wind vectors over the ocean. Even though SASS made measurements of σ^o over land and ice regions, the application of this data has been limited due to the low (50 km) resolution of the measurements.

A new technique for generating high resolution (5 km) images of surface radar backscatter characteristics is detailed in a companion paper [1]. The method utilizes overlap in the measurement cells from subsequent orbits over the region of interest and combines them using signal processing techniques in order to form high-resolution estimates of backscatter coefficients. In this paper we apply the reconstruction method to SASS data for the study of Greenland's ice sheet. We present a time series of the radar backscatter images over Greenland covering the time period July-September 1978. The images provide an island-wide view of the ice sheet which dramatically show the areal extent of the summer melt. Little change was observed in central Greenland.

While our interpretation of the imagery is necessarily preliminary, our goal is to stimulate interest in the use of SASS, NSCAT, and other EoS-era scatterometer data for ice studies. The medium-scale scatterometer images will provide frequent island-wide observations permitting precise measurements of the seasonal extent of the summer melt. Because the polar regions are particularly sensitive to climate, use of scatterometry data may provide us with an efficient way of monitoring large-scale variations in arctic ice and facilitate our understanding of global climate change.

INTRODUCTION

The Seasat-A scatterometer was designed to make 50 km (nominal) resolution measurements of σ^o. The antenna design allowed these measurements to be taken at two azimuth angles over a pair of 500 km wide swaths separated by a 400 km nadir gap. Acquired over global oceans, these σ^o measurements were used to infer the near-surface wind vectors using a geophysical model function relating σ^o and the surface wind velocity and direction.

While the 50 km resolution was adequate for ocean studies, the low resolution has limited the application of the data over land and ice. The primary application for σ^o measurements over land has been instrument calibration. For this, homogeneous regions of tropical rainforest were observed in order to verify and correct the SASS instrument calibration [2].

In this paper we apply a new method for generating high resolution SASS images [1] to the measurements acquired over Greenland during the ill-fated three month mission of Seasat-A. The technique permits generation of images with a resolution as good as 4-5 km from the 50 km resolution SASS measurements. While the resulting images can only be considered "high" resolution when compared to the inherent resolution of the scatterometer, they can nonetheless be very useful for the study of the Greenland ice sheet.

In the sections following, we briefly describe our imaging technique and its limitations. Next, we exhibit a single high resolution SASS image of Greenland with a brief commentary. We then examine a time series of radar backscatter for a few 1° study areas. Finally, we conclude with a SASS image time series showing the entire island in which the seasonal change over the time period of July-September, 1978 is dramatically evident.

THE IMAGING TECHNIQUE

The Model for $\mathcal{A}$ and $\mathcal{B}$. SASS made both vertically and horizontally polarized measurements of σ^o at several azimuth and incidence angles. Ignoring any azimuthal modulation of σ^o (as we did), σ^o over land and ice is a function of the measurement incidence angle (θ). For many surfaces, a linear model relating σ^o (in dB) to the incidence angles between 20° and 55° can be used, i.e. [2]

$$10\log_{10}\sigma^o(\theta) = \mathcal{A} + \mathcal{B}\ (\theta - 40°),$$

where the coefficients $\mathcal{A}$ and $\mathcal{B}$ depend only on the surface characteristics. $\mathcal{A}$ can be thought of as the *incidence angle normalized* σ^o, while $\mathcal{B}$ describes the incidence angle dependence of σ^o. Because of the wide diversity of incidence angles, we use the $\mathcal{A}$ and $\mathcal{B}$ coefficients in lieu of σ^o.

The Tradeoffs. As described in [1], our high resolution imaging technique uses multiple overlapping measurements of σ^o and ground processing techniques to effectively estimate $\mathcal{A}$ and $\mathcal{B}$ at a resolution better than the intrinsic resolution of the σ^o data. However, the resolution enhancement technique has a penalty: the noise in the $\mathcal{A}$ and $\mathcal{B}$ images increases as the resolution increases. In practice, a tradeoff must be made between resolution and the noise level. To minimize noise and still produce high resolution, multiple orbit passes of the target are required. During this *imaging time interval* the calibration of the instrument itself and the radar characteristics of the target must remain constant. Thus a tradeoff between the imaging time interval and resolution must be made.

The Assumptions. Prerequisites for successful use of the new image reconstruction technique include the following. We note that these assumptions may be relaxed when applying the method to suitably modified future scatterometers since multiple orbit passes may not be required [3].

1. The instrument calibration remains stable over the data acquisition interval. Based on measurements of the Amazon rainforest (which exhibits limited seasonal variation), the calibration stability of SASS was acceptable.
2. Azimuthal modulation can be ignored. Examination of the Greenland data indicated some azimuthal modulation may be present in the σ^o measurements. However, in order to apply the SIRF algorithm to the Greenland data, we have disregarded it. A future examination of azimuthal modulation over Greenland ice is planned.
3. The effects of surface topography are small and may be neglected. Surface slope affects the local incidence (and azimuth) angles which, in turn, may effect the estimates of $\mathcal{A}$ and $\mathcal{B}$. However, $\mathcal{B}$, which describes the incidence angle dependence of σ^o is relatively small over Greenland ice (e.g. $0.1 \le \mathcal{B} \le 0.22$). Considering the small value of $\mathcal{B}$, the topographic influence on the $\mathcal{A}$ values is small.
4. The $\mathcal{A}$ and $\mathcal{B}$ parameters for the target region remain constant over the imaging time interval. For a sufficiently short imaging time interval this assumption is justified. However, in applying the reconstruction method to SASS data over Greenland, the imaging time interval must be very long (days to weeks) to accumulate sufficient measurement overlap for creating low noise 4-5 km resolution imagery.

   We have observed both long-term and short-term changes in $\mathcal{A}$ and $\mathcal{B}$ in some regions over the 3 month period. During July some regions along the ice sheet margin exhibited large spatial σ^o changes. Unfortunately, SASS provided only very limited time-of-day measurement diversity and an ongoing

91-72810/92$03.00 © IEEE 1992

examination of diurnal change is presently inconclusive. In generating images presented below, diurnal variations were not considered. Images in the time series were generated using two weeks of SASS data. In contrast, Figure 1 was generated using the entire last month of SASS data. During this final month of the mission, little change in σ^o was observed.

The Data Selection Criteria. The SASS σ^o measurements spanned an incidence angle range of 0° to 70°; however only measurements with incidence angles between 20° and 55° were used in this study. In addition, measurements with excessive noise (i.e., those with normalized standard deviation (K_p) greater than 100%) were discarded. Likewise, data from orbits with large spacecraft attitude errors were not used. The interested reader is invited to review [2] for a detailed description of SASS data anomalies and the rationale for selecting and excluding orbits with excessive error.

The Image Reconstruction. The scatterometer image reconstruction with filtering (SIRF) algorithm described in [1] provides high resolution (4 km) images of $\mathcal{A}$ and $\mathcal{B}$ from the 50 km SASS resolution data. Images were generated separately for both vertically and horizontally polarized σ^o measurements. In this paper we present only images generated from vertically-polarized σ^o measurements. The horizontally-polarized images are similar in appearance with some differences in details.

As mentioned in [1], σ^o measurements spanning a sufficient range of incidence angles are required to estimate both $\mathcal{A}$ and $\mathcal{B}$. As a rule, each high resolution element (pixel) over Greenland was generally observed with a wide diversity of incidence angles. For the exceptions, a $\mathcal{B}$ value was assigned to the pixel rather than estimated. In these cases, the assigned $\mathcal{B}$ was the time averaged $\mathcal{B}$ value over the mission. Since the $\mathcal{B}$ values are small, this introduces only small errors in the $\mathcal{A}$ estimate.

The Greenland Image. Using SASS data and the SIRF algorithm, we generated a high resolution (4 km) image of $\mathcal{A}$ for Greenland using the last month of data (Figure 1). In contrast to the $\mathcal{A}$ image, the corresponding $\mathcal{B}$ image (not shown) has only limited detail. We note the very bright (-4 dB) response in the dry snow zone in north-central Greenland as well as the bright (-3 to -1 dB) band girdling the margin of the ice sheet. Although the interpretation of this feature is unknown, it may be due to the formation of ice lenses.

SPATIAL AND TEMPORAL BACKSCATTER VARIATION

Temporal Variation. To illustrate the spatial and temporal variation in $\mathcal{A}$ we present plots of $\mathcal{A}$ versus Julian day (1978) in Figure 2. To generate these plots, the σ^o records for two 1° x 1° regions along a meridional transect located approximately 66° N were extracted from the SASS data set. An average $\mathcal{B}$ value determined by regressing σ^o on θ over the three month data set. This average $\mathcal{B}$ was then used to compute the $\mathcal{A}$ coefficients for each 1° x 1° study area from the σ^o measurements.

The significant change in $\mathcal{A}$ through the time sequence is apparent. While there is a significant variation over the 3 month data set, the change over any 1-2 week period is relatively small, allowing us to confidently generate a time series of high-resolution images using 2 week segments of data (see below). We attribute the low $\mathcal{A}$ value corresponding to July in Figure 2 to the existence of melt ponds and saturated snow during the summer. These apparently begin to disappear in August.

Sample plots of σ^o versus θ for region 2 are presented in Figure 3. For each plot, linear regression was used to compute $\mathcal{A}$ and $\mathcal{B}$. Figure 3a is for Julian days 207 through 214 (during the summer season). We note the wide scatter in the data around $\mathcal{A}$ = -11.1 and $\mathcal{B}$ = -0.148. Figure 3b, showing σ^o after the summer season (Julian days 245 through 283) has much less scatter with an average $\mathcal{A}$ value approximately 10 db higher ($\mathcal{A}$ = -1.8, $\mathcal{B}$ = -0.192). The change in the mean $\mathcal{A}$ value is undoubtedly due to refreezing along the ice sheet margin. The accompanying decrease in backscatter variance likely corresponds to the disappearance of saturated snow and melt ponds.

Greenland Image Time Series. Having determined the low variability of σ^o over short time intervals, the series of $\mathcal{A}$ images shown in Figure 4 was then generated. Each image used a two week time segment of SASS data separated sequentially by two calendar weeks. The seasonal variation is clearly evident in this image time series with the dramatic variation in $\mathcal{A}$ along the ice sheet margins. This variation is attributed to the subsequent refreezing after the summer melt. Over central Greenland, which exhibits a very high radar backscatter at 14.6 GHz, very little change was in the three month data set.

Along the margin of the ice sheet, particularly along the western and southeastern coasts, significant changes in $\mathcal{A}$ were observed from early July through mid August. As the season progressed through July, this melt zone margin, marked by reduced backscatter and large spatial and temporal variability in σ^o, was first observed to advance further inland and then retreat coastward in early August. Until September, these regions exhibited significant increases in the mean $\mathcal{A}$ as well as remarkable spatial homogeneity. By late September, these regions had extremely large (-5 to -3 dB) $\mathcal{A}$ values, surpassing the remarkably bright central dry snow region. In the buffer zone between these two extremes, $\mathcal{A}$ was reduced 4 to 6 dB. Significant backscatter brightness changes were also noted along the coastal regions.

The large change in $\mathcal{A}$ along the entire ice sheet margin during July is attributed to the growth of surface melt ponds. The formation in early August of a bright band several degrees east of the southwest coast which was separated from the bright central regions of the sheet by a darker melt band, is not clearly understood.

CONCLUSION

We have utilized low resolution SASS *Ku*-band measurements of σ^o to compute high resolution images of $\mathcal{A}$ and $\mathcal{B}$. Though these measurements are only medium-scale (4 km), they provide an island-wide view of the ice conditions of Greenland. A time series of these images clearly delineates the areal extent of the summer melt region.

Even though SASS data is over a decade old it is nonetheless an effective tool for validating the high resolution imaging technique. The technique can also be applied to ERS-1, future scatterometers, and other sensors. With low-cost modifications to future planned scatterometers such as the NASA Scatterometer (NSCAT), the imaging resolution can be further improved to as high as 1-2 km [3]. Coupled with very frequent revisits and multiple-incidence angle observations, this will significantly enhance the application of scatterometer data to the study of continental and sea ice. In particular, the multiple-incidence angle measurements may be used to infer ice condition/age, melt patterns and snow cover. Furthermore, since the scatterometer is an all-weather active sensor, it can make continuous measurements throughout the year. The proposed modifications are summarized in [3].

ACKNOWLEDGEMENTS

We wish to acknowledge the support of the NASA Headquarters programs in Physical Oceanography (Gary Lagerloef and David Adamec) and Polar Sciences (Robert Thomas). The SASS GDR data was obtained from the NASA Ocean Data System at the Jet Propulsion Laboratory/California Institute of Technology.

REFERENCES

[1] Long, D.G., P.T. Whiting and P.J. Hardin, "High-Resolution Land/Ice Imaging Using Seasat Scatterometer Measurements", *Proceedings of the International Geoscience and Remote Sensing Symposium*, Houston, TX, May 1992.

[2] Bracalente, E. and J. Sweet, "Analysis of Normalized Radar Cross Section (σ^o) Signatures of Amazon Rain Forest Using Seasat Scatterometer Data", *NASA Technical Memorandum 8779*, NASA NTIS, 1984.

[3] Long, D.G., and P.J. Hardin, 1992. "High Resolution Imaging of Land/Ice using Spaceborne Scatterometry Part II: Vegetation Studies of the Amazon and Future Applications." Submitted to *IEEE Transactions on Geoscience and Remote Sensing.*

Figure 1. An $\mathcal{A}$ image generated using vertically-polarized σ° measurements made during the last month of the SASS mission.

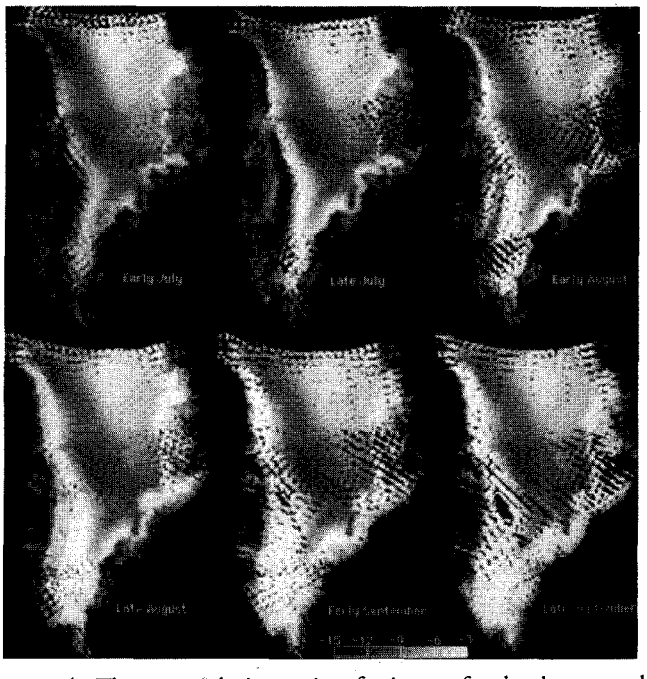

Figure 4. The two week time series of $\mathcal{A}$ images for the three month SASS mission. Each image used two weeks of vertically-polarized σ° measurements.

Figure 2. The $\mathcal{A}$ time series for the 1° x 1° rectangular study regions. (a) Region 1 centered on 66.5° N 49° W. (b) Region 2 centered on 66° N 47° W.

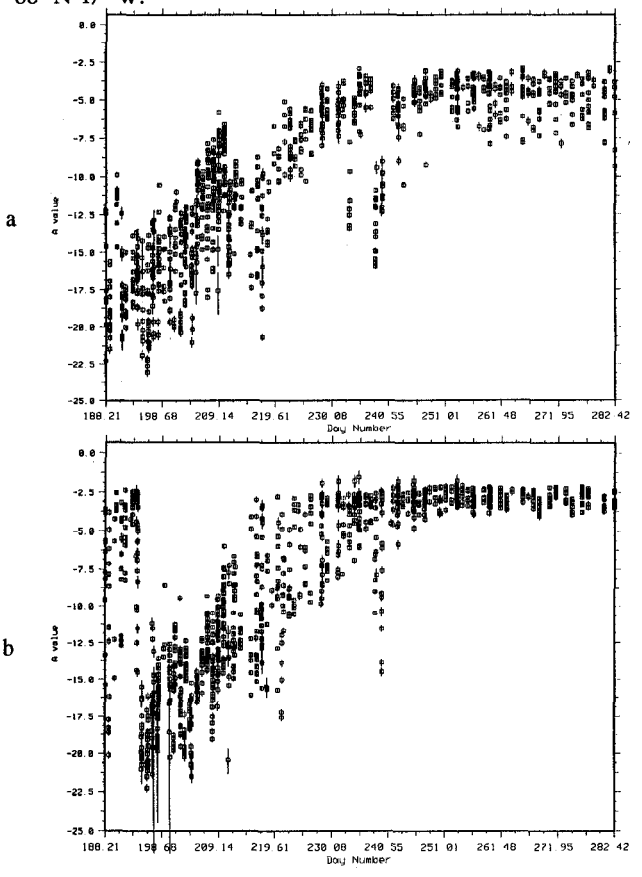

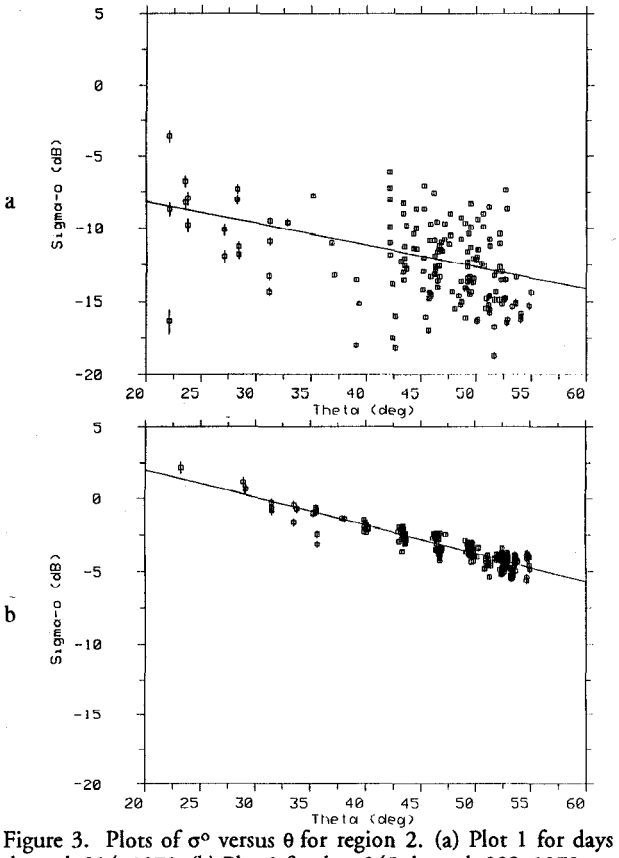

Figure 3. Plots of σ° versus θ for region 2. (a) Plot 1 for days 207 through 214, 1978. (b) Plot 2 for days 245 through 283, 1978.